Extended Abstracts of the 20th (1988 International) Conference on Solid State Devices and Materials, Tokyo, 1988, pp. 97-100

High-Dose and MeV-Energy Ion Implantation into Si for Buried-Layer Formation

Tadashi SUZUKI, Masao TAMURA, Kiyonori OHYU and Nobuyoshi NATSUAKI

Central Research Laboratory, Hitachi, Ltd.,

Kokubunji, Tokyo 185, Japan

MeV B-, P- and As-implanted Si with a dose of 5 x $10^{15}/cm^2$ are investigated in terms of electrical activation, defect distribution and impurity profiles. Defect-free regions are obtained from the surface to a depth of 1.5 μm after 1000-1100℃ annealing, which are independent of the existence of buried-amorphous layers in as-implanted samples. In addition, important role of oxygen on defect formation is clarified. These results provide a useful information for forming buried layers with a high concentration.

1. INTRODUCTION

Recently, MeV-energy ion implantation has been intensively studied for various device applications. Some useful applications such as latch-up protection[1-2] and soft-error reduction[3] in CMOS have been already demonstrated in LSI level for low-dose implantation ($\leq 10^{13}/cm^2$). However, for the application of high-dose implantation ($\geq 10^{15}/cm^2$) such as buried subcollector formation in bipolar transistors, only a few reports have been published[4]. This is because damage formation and annealing behavior of high-energy implanted layers with high doses have not been understood yet.

In this paper, crystallographic characteristics of B-, P- and As-implanted Si (energy $\geq$ 1 MeV, dose $\geq 1 \times 10^{15}/cm^2$) are comprehensively studied to optimize the conditions for buried-layer formation. In particular, influences of buried-amorphous layers and bulk material natures (CZ or FZ) upon residual defect distributions are investigated.

2. EXPERIMENTAL PROCEDURES

Two MeV B^+ and P^+, amd 3 MeV As^+ ions were implanted into (100) and (111) Si wafers with a dose of 5 x $10^{15}/cm^2$ as a function of beam current (0.4-4 μA) using a TANDEM machine. The implanted area was 87 cm^2 for all the wafers. To investigate the effect of oxygen atoms on defect formation during annealing, both CZ and FZ substrate material types were used. After implantation, samples were annealed in dry N_2 at temperatures ranging from 450 to 1100℃ in a conventional furnace tube. Secondary defect distributions and annealing behavior were studied mainly by cross-sectional TEM (XTEM) observations. SIMS measurements were used to obtain the depth distribution for implanted impurities and oxygen atoms. For some samples, sheet-resistance measurements were also performed.

3. RESULTS AND DISCUSSION

3.1 Effect of Dose Rate

Figure 1 shows typical XTEM micrographs, which shows the dose-rate effect on the primary defect formation and distribution, in P and As implanted Si. The present implanter was not equipped with a special wafer cooling system. In high-dose implantation, primary

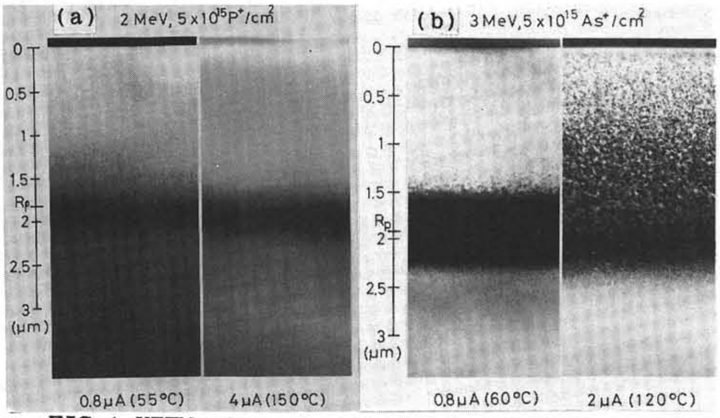

FIG. 1 XTEM micrographs showing dose-rate effect on the primary defect formation in P and As implanted Si.

damage formation conditions such as formation of buried-amorphous layers can be easily controlled by changing the beam current. This is because substrate temperature is precisely controlled by beam current. We estimated temperature rise during implantation based on radiation limited heat-flow under a emissivity value of 0. 35. Estimated temperatures are indicated in each micrograph. In P implantation (Fig. 1(a)), no buried-amorphous layer was observed in either implanted layer even for doses as high as 5 x $10^{15}/cm^2$, although about 0. 2 μm-width black band layers (damage clusters) are formed at around Rp (projected range) depth of 2 MeV P ions in Si. In contrast, buried-amorphous layer formation occurs for the low beam current case (0. 8 μA) in 3 MeV As implantation (Fig. 1(b)). In no buried-amorphous layer formed sample (2 μA), small dislocation loop formation is seen from a 0. 1 μm depth below the surface due to growth of damage clusters caused by temperature rise during implantation.

Next, residual defect distributions after annealing are shown for As case. Figure 2 shows XTEM micrographs of 3 MeV As implanted and annealed (1000℃, 60 min) samples for both initially amorphized (a) and non-amorphized (b) cases. In a non-amorphized sample, a simple dislocation entanglement band exists at depths between about 2 and 3 μm depth. However, an amorphized sample contains three different defect bands. The first band is a dislocation line group in the region between 1. 5 and 2 μm depth. The second one is a stripe composed of dislocation loops. The stripe position matches the lower amorphous/crystalline (a/c) interface in the as-implanted layer. The final defect band consists of high-density dislocation loops (2. 4-2. 8 μm below the surface). Thus, we have concluded that the nature and distribution of residual defects depend on whether buried-amorphous layers are initially formed. However, no defects were noted between the surface and depths of about 1. 5 μm, which were independent of the existence of buried-amorphous layers in as-implanted samples. This is an important consideration for device applications of this technique.

3. 2 Effect of Substrate Materials

In this section, the effect of substrate material on electrical recovery of implanted amorphized layers and residual defects after annealing are discussed. Figure 3 shows isochronal annealing characteristics (15 min) of sheet resistance for 3-MeV As implanted samples. For all the samples, buried amorphous layers were formed in as-implanted samples, except for one case indicated in the figure. The sample which does not contain a

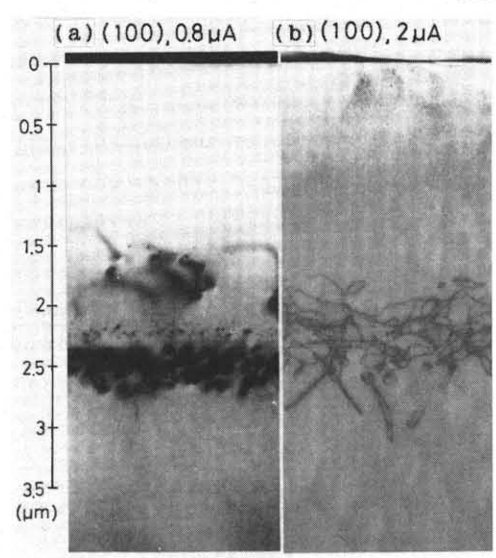

Fig. 2 XTEM micrographs of 3 MeV As implanted and annealed Si for initially amorphized(a) and non-amorphized(b) cases.

buried amorphous layer shows a gradual decreasing resistance with the increased annealing temperature throughout all the temperature range. In contrast, the other three samples containing buried amorphous layers show abrupt resistance decreases in the temperature range between 550 and 650℃, depending on the bulk material nature. In these samples, CZ (111) Si electrical recovery is slowest and matches with the slowest solid-phase-epitaxy (SPE) regrowth velocity. The different reduction of sheet-resistance between FZ and CZ (100) materials is due to the different oxygen contents of the materials. In the CZ Si used in the present experiment, about $1x10^{18}/cm^3$ oxygen atoms are included. Therefore, these oxygen atoms retard the SPE recovery of a buried amorphous region, resulting in delaying the recovery of electrical activation.

After high-temperature annealing at 1000-1100℃, almost all the implanted ions become electrically active. However, defect natures and morphology strongly depend on both substrate natures and ion species. In particular, severe interactions between defects and oxygen atoms in CZ crystals are observed.

Figure 4 shows a comparison of defect densities in CZ and FZ (100) Si implanted with 2 MeV, $5 \times 10^{15} B/cm^2$ ions followed by 1000℃ 60 min annealing. Apparently, dislocation

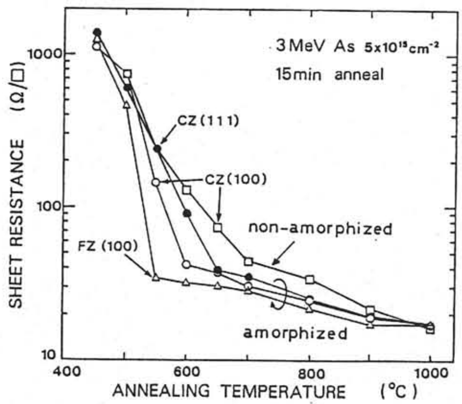

FIG. 3 Isochronal annealing characteristics of sheet resistance in 3 MeV As implanted samples.

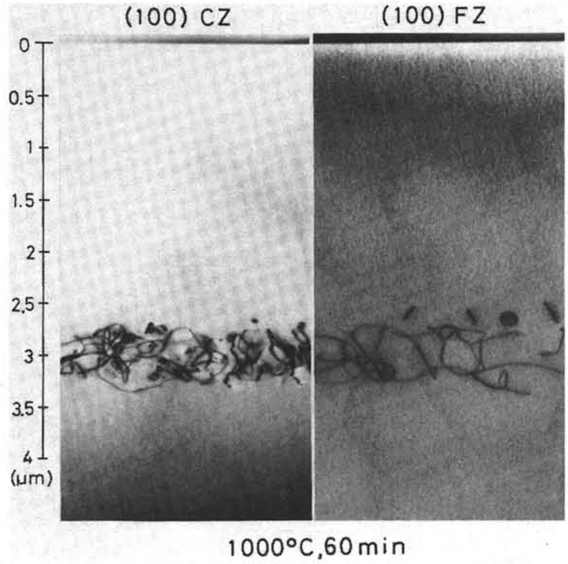

FIG. 4 XTEM micrographs of 2 MeV B implanted CZ and FZ (100) Si after annealing.

density in FZ Si is much lower than that in CZ Si. Higher dislocation density in CZ Si is attributed to the pinning effect of oxygen atoms on defects. Figure 5 shows depth distribution profile changes of oxygens as a function of annealing temperature. This figure clearly indicates that an oxygen pile-up phenomenon begins at 800℃. Annealing at 1000℃ results in a sharp oxygen concentration peak at about 3 μm from the surface. The oxygen atom pile-up regions strictly coincides with defect band regions in Fig. 4. Under these annealing conditions (1000℃, 60 min), the oxygen diffusion length is estimated to be 2-3 μm. Therefore, we can conclude that high-temperature annealing

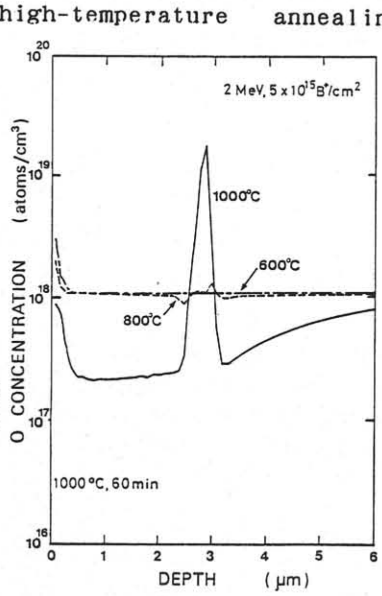

FIG. 5 Depth profiles of oxygens in 2 MeV B implanted and annealed CZ Si as a function of annealing temperature.

induces the out-diffusion of oxygens towards the surface and the oxygen interacts with defect bands and pins defects during diffusion.

Similar features were also observed in P and As implanted layers. Depth profiles of As and oxygen atoms in As implanted CZ (100) Si are shown in Fig. 6 after 1000℃ 60 min annealing. There are two oxygen peaks at different depths. We do not think that these oxygen peaks originate from interactions with As atoms, since the respective peak positions are at different depths as seen in the figure. Accordingly, these two oxygen peaks are considered to be induced by the oxygen gettering at the defect bands in Fig. 2(a) during annealing process. The deeper oxygen peak (about 2.4 μm below the surface) certainly coincides with the third defect band which consists of high-density dislocation loops. However, no visible defect band exists at a shallower position of an oxygen peak at around 1.2 μm. A similar oxygen peak at a surface-side position (1-2 μm) was also detected in P implanted and annealed layers, although peak value ($\sim 2 \times 10^{18}$ atoms/cm^3) was slightly lower than that in As case ($\sim 3 \times 10^{18}$ atoms/cm^3). However, this second peak was not observed in B implanted samples as shown Fig. 5.

From these results, the cause of oxygen pile-up at shallow depths may be due to interactions with point defects generated along individual ion tracks and not with secondary defects. These interactions becomes dominant with the increase of ion mass. As a result, a pile-up oxygen peak becomes higher in the regions where heavier ions were passed. An interaction between oxygens and point defects in the above regions are considered as follows : At the first stage, an interstitial oxygen atom will combine with a point defect, resulting in the formation of, e.g., A-center (vacancy-oxygen complex). Then, such complexes further interact and coalesce each other with the progress of thermal treatment. Finally, the precipitation of oxygens will occur. In fact, after very high-temperature annealing at 1300℃, many precipitates which are thought to be oxygens are observed.

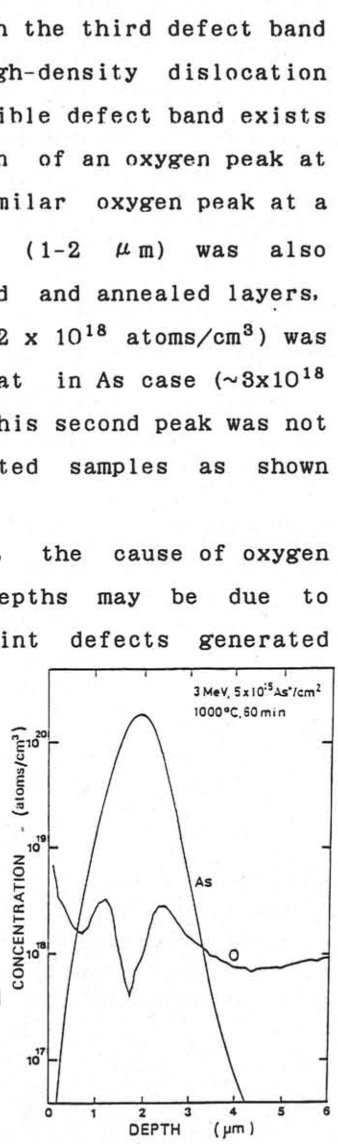

FIG. 6 Depth profiles of arsenic and oxygen atoms in 3 MeV As implanted and annealed CZ Si.

4. CONCLUSION

MeV B-, P- and As-implanted Si with a dose of 5 x 10^{15}/cm^2 were investigated in terms of electrical activation, defect distribution and impurity profiles. Defect-free regions were obtained from the surface to a depth of about 1.5 μm after 1000-1100℃ annealing, which were independent of the existence of buried-amorphous layers in as-implanted samples. However, oxygens were precipitated in near-surface region in the case of CZ Si. Consequently, it is needed to pay a close attention in forming active devices in these regions. In addition, important role of oxygen on defect formation was clarified.

REFERENCES

1) K. W. Terrill et al., Appl. Phys. Lett., 45, 977 (1984).

2) K. Ohyu et al., 7th Int'l Conf. Ion Implantation Technology, Kyoto, p. 191, 1988.

3) Y. Matsuda et al., Extended Abstracts of 19th SSDM, 23 (1987).

4) M. Doken et al., Tech. Dig. IEDM81, 586 (1981).